ISSN: 2229-6948(ONLINE)
DOI: 10.21917/ijct.2026.0560

RAY-TRACING-BASED MODELLING AND CHARACTERIZATION OF TERAHERTZ CHANNELS FOR 6G WIRELESS COMMUNICATIONS

R. Rajaganapathi, V. Rajakani, K. Karthick Babu and P. Dinesh
Department of Electronics and Communication Engineering, Anjalai Ammal Mahalingam Engineering College, India

Abstract

The unique properties of terahertz (THz) waves were examined, particularly in contrast to lower-frequency bands, highlighting the effects of weather conditions and material surface roughness on THz signal propagation. To address modeling challenges, the study introduced a ray-tracing (RT) approach to refine the 3D environmental model and material electromagnetic properties using minimal channel measurement data. These calibrated parameters were then applied to broader scenarios, reducing reliance on extensive measurements. Key channel characteristics—such as path loss, shadow fading, Rician K-factor, delay spread, angular spread, and Doppler effects in mobile settings—were analyzed. The research explored two distinct 6G THz use cases: indoor desktop wireless links and outdoor vehicular communications, with the latter incorporating weather-related impacts. These findings offer valuable insights for designing and assessing THz communication systems.

Keywords:

THz Communication, Wave Propagation, Ray-Tracing

1. INTRODUCTION

With the advancement of mobile communication systems, the need for real-time connectivity and high data rates has grown to support various online applications. International organizations have addressed this with standards like LTE (3GPP), IEEE 802.11 (WLAN), and IEEE 802.15 (WPAN).

Millimetre wave (mmWave) communication enhances 5G capacity through technologies such as MIMO, CoMP, and Carrier Aggregation, achieving speeds of several Gbit/s. However, available bandwidth in microwave and mmWave ranges is limited, with no more than 10 GHz typically accessible.

6G aims to build on 5G, transforming traditional IoT into intelligent IoT. Research by ITU, 3GPP, and CCSA has already begun, targeting standardization around 2030. To achieve future data rates above 100 Gbps, terahertz (THz) frequencies (0.1–10 THz) are gaining attention as a key enabler. Positioned between mmWave and visible light bands, the THz spectrum offers high capacity and low interference, and can penetrate smoke, dust, and non-metallic materials, making it suitable for secure and reliable communication.

Accurate channel modeling is essential for efficient THz communication system design. These models integrate theory, measurement, and simulation. The IEEE 802.15 TG3d standard defines key indoor and outdoor THz communication scenarios. Additionally, ITU has proposed using 0.22 THz for satellite-to-satellite communication. While satellite modeling remains largely in simulation due to hardware limits, ground-based THz modeling has seen more progress.

Random channel models, such as 3GPP's SCM and WINNER, are built on empirical data and enable both link- and system-level simulation. Geometry-based stochastic models (GBSMs) use probabilistic distributions and simplified physical assumptions to simulate channel behaviour.

At higher frequencies, like mmWave, practical channel measurements are limited due to beam alignment issues and coherence time. Ray tracing (RT) simulations have emerged as a reliable method to overcome sparse measurement datasets and provide accurate characterization.

For THz, measurement challenges are more severe. Although various studies have been done on on-chip, indoor, and vehicular channels, available datasets are limited. RT, based on geometric optics, offers a promising solution. It's already used to model realistic propagation scenarios in indoor and transportation environments.

RT simulations help estimate key channel characteristics—path loss, fading, delay spread, Doppler shift—while considering additional losses from atmospheric absorption and weather effects like fog and rain. This paper contributes a ray-tracing-based framework incorporating meteorological effects and surface roughness, validated through two case studies: indoor wireless and intelligent vehicle networking.

2. TERAHERTZ WAVE PROPAGATION CHARACTERISTICS

2.1 EFFECTS OF METEOROLOGICAL FACTORS

Compared with low-frequency wireless communication below 100 GHz, terahertz wireless channels are more susceptible to different meteorological factors, mainly including atmospheric gases, clouds, rain, snow, etc. To meet the requirement of full coverage of 6G air space integration, ground communication networks also need non ground communication networks for assistance, especially for outdoor scenarios such as drone communication, satellite ground communication, vehicle networking communication, etc. The attenuation caused by molecular absorption and particle scattering of these meteorological factors cannot be ignored in the analysis of terahertz channel characteristics.

2.1.1 Absorption Attenuation of Atmospheric Molecules:

The attenuation of atmospheric molecule absorption is caused by the absorption of electromagnetic wave energy by atmospheric molecules. Some of the excited molecules in the atmosphere vibrate at a certain frequency, resonate with electromagnetic waves, and some electrons undergo energy level transitions. The energy of electromagnetic waves is converted into kinetic energy of molecules [28], that is, the energy of electromagnetic waves is lost. In the terahertz frequency band, it is mainly affected by oxygen and water vapor, as well as temperature, pressure, and altitude. ITU-R P.676-11 Recommendation [29] provides an atmospheric absorption attenuation model, which can be applied

up to 1 THz. The absorption loss (in dB/km) of atmospheric molecule absorption attenuation can be expressed as

$$\gamma_a(f) = \gamma_o(f) + \gamma_w(f) \tag{1}$$

Where, γ_0 is the absorption attenuation of oxygen molecules under dry air conditions, and γ_w is the characteristic attenuation of water vapor molecules in the atmosphere, both of which are related to frequency f and measured in dB/km. The absorption attenuation of atmospheric molecules in standard atmospheric environment, oxygen, and water vapor is shown in Fig.1. From the overlapping part of the curve in Fig.1, it can be seen that when the frequency is above 100 GHz, the total absorption attenuation in the standard atmospheric environment is equivalent to the molecular absorption attenuation of water vapor, indicating that the absorption attenuation of water vapor dominates in the terahertz frequency band. The absorption of atmospheric molecules can also define important transport windows (as shown in Fig.1). Choose different transmission windows for different applications, such as meteorological remote sensing, which requires the use of sensitive absorption peaks to improve remote sensing accuracy; For communication systems, it is necessary to apply a transmission window with minimal absorption and attenuation of atmospheric molecules.

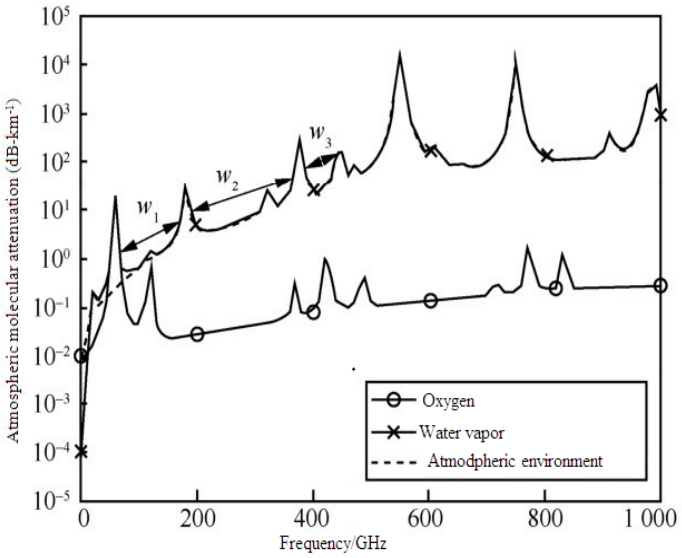

Fig.1. Atmospheric molecular attenuation

2.1.2 Particle Scattering Attenuation:

When terahertz communication is applied in outdoor scenarios, it is not only necessary to consider the absorption of atmospheric molecules, but also the scattering effect of meteorological particles such as fog, rain, and snow in the actual communication environment. When terahertz electromagnetic waves encounter suspended particles during transmission, their energy scatters out of the propagation path, causing attenuation of radio wave energy.

Fog is also considered a cloud obstructed by the ground, with a similar microphysical structure to clouds, and often appears in areas with high water vapor content such as mountainous areas and beaches. The parameter characterization of fog is usually based on its liquid water density, optical visibility, and droplet size distribution. Typically, the density of liquid water is 0.05 g/m3 for medium fog (visibility of approximately 300 m) and 0.5 g/m3 for dense fog (visibility of approximately 50 m). According to ITU-R P.840-7 recommendation [30], for small particles such as clouds and mist, the Rayleigh approximation method is used to calculate the attenuation of clouds and mist

$$\gamma_{fog}(f,T) = K_l(f,T)M \tag{2}$$

Where, $K_l(f,T)$ is the attenuation coefficient of liquid water ratio; M is the density of liquid water; F is the operating frequency, measured in GHz; T is the temperature of liquid water, measured in K. The expression for $K_l(f,T)$ (in dB·km^{-1}/(gm^{-3})) is

$$K_l(f,T) = \frac{0.819}{\varepsilon''(1+n^2)} \tag{3}$$

$$\eta = \frac{2+\varepsilon'}{\varepsilon''} \tag{4}$$

Where, ε'and ε'' are the real and imaginary parts of the relative dielectric constant of water.

The attenuation of terahertz electromagnetic waves propagating in rainy media increases with the increase of rainfall. In ITU-R P.838-3 Recommendation [31], for a given precipitation rate R (in mm/h), regardless of the amount of rainfall, the attenuation caused by rainfall increases exponentially. The attenuation model (in dB/km) can be expressed as

$$\gamma_{Rain} = kR^{\alpha} \tag{5}$$

where, k and α are functions of operating frequencies ranging from 1 GHz to 1 THz, and they are also influenced by parameters such as temperature, polarization mode, and height. For all paths, the calculation methods for k and α for linear polarization and circular polarization are as follows:

$$k = \frac{k_H + k_V + (k_H - k_V)\cos^2\theta\cos 2\tau}{2} \tag{6}$$

$$\alpha = \frac{k_H\alpha_H + k_V\alpha_V + (k_H\alpha_H - k_V\alpha_V)\cos^2\theta\cos 2\tau}{2k} \tag{7}$$

Where, θ is the pitch angle of the path, and τ is the polarization angle relative to the horizontal direction. The frequency dependent values of k_H, k_v, as well as α_H and α_v can be obtained from ITU-R P.838-3 recommendation [31]. In addition, ITU-R Proposal P.837-7 [32] provides annual statistical data on global rainfall parameters, with rainfall provided by digital maps and corresponding latitude and longitude information. The R0.01 given in the proposal represents that the target area will only exceed this rainfall amount 0.01% of the time. ITU-R P.530-17 Recommendation [33] further provides for calculating the effective path length based on the actual path length, thereby determining the path loss caused by rainfall

$$Att_{Rain} = \gamma_{Rain}d_{eff} = \gamma_{Rain}d_r \tag{8}$$

Where, d_{eff} is the effective path length, and the estimated value r of the distance coefficient is

$$r = \frac{1}{0.477d^{0.633}R_{0.01}^{0.073\alpha} - 10.579\left(1-e^{-0.024d}\right)} \tag{9}$$

The recommended maximum value for r is 2.5. If the molecule in Eq.(9) is less than 0.4, then r=2.5 is chosen.

Due to limited research on the path loss caused by snowfall, ITU-R does not have a relevant recommendation to provide a model for predicting snow attenuation. Snowflakes have different shapes and surface structures, with typical structures being columnar, needle shaped, and dendritic. They are mainly composed of air, liquid water, and ice crystals. Due to the size of snowflakes being comparable to terahertz wavelengths, reference [34] indicates that under the same precipitation rate, the attenuation caused by snowfall is three times that of rainfall. Reference [35] conducted measurements of snowfall, in which the transmitter was located under the roof and the receiver received electromagnetic waves ranging from 50 to 300 GHz at a distance of 8 meters from the transmitter. By comparing the results with measurements on sunny days under the same configuration, the additional attenuation under snowfall conditions was obtained. Although there have been some experimental studies on fog, rain, and snow weather in the terahertz frequency band, there is a lack of research on channel measurement, especially in adverse weather conditions that may damage sensitive measurement equipment. The ray tracing simulator can be regarded as an effective way to expand the channel database. By embedding atmospheric molecule absorption and particle scattering attenuation models into the ray tracing simulator, it can replace measurement data under adverse weather conditions and achieve research on outdoor ground wireless channels under different weather conditions.

2.2 ROUGH SURFACE BACKSCATTERING CHARACTERISTICS

In the multipath composition of radio wave propagation, in addition to the dominant LoS, the reflection link will also play an important role in ensuring the robustness of communication. The specular reflection of an ideal smooth surface can still be characterized by the classical Fresnel reflection coefficient. But as the frequency of electromagnetic waves increases and the wavelength becomes shorter, the surface that could have been considered smooth at low frequencies becomes rough in the terahertz frequency range, and the scattering that occurs on its surface weakens the energy in the direction of specular reflection. The smoothness of the material surface can be determined by the Rayleigh criterion, that is

$$h_c = \frac{\lambda}{8\cos\theta_i} \tag{10}$$

Where, θ_i is the incident angle, and λ is the wavelength of the electromagnetic wave. Assuming the maximum height difference of the material surface undulation is h_0, if $h_0<h_c$, it is considered that the material surface is smooth; On the contrary, it is considered that the surface of the material is rough. In order to evaluate the loss of specular reflection power due to the roughness of the material surface, the Fresnel model was modified by the scattering loss factor ρ_s [36], that is

$$\rho_s = e^{-g/2} \tag{11}$$

Among them

$$g = \left(\frac{4\pi\sigma_h \cos\theta_i}{\lambda}\right)^2 \tag{12}$$

Where, σ_h is the mean square value of the surface height. From equations (11) and (12), it can be seen that the magnitude of ρ_s depends on the wavelength and incident angle of the electromagnetic wave. As the surface roughness, frequency, and incident angle increase, the loss factor increases and the energy attenuation of specular reflection increases. [37] validated the accuracy of the model by measuring materials with three different roughness levels. This model is suitable for rough surfaces with a height distribution that follows a Gaussian distribution and can be applied to the vast majority of common materials.

Modeling rough material surfaces with Gaussian distribution is the first step in studying diffuse scattering on rough surfaces. Its statistical characteristics mainly include root mean square height σ h and correlation length l, which are usually modeled using Monte Carlo method [38]. Monte Carlo method, also known as linear filtering method, is based on filtering the frequency using power spectrum, and then performing inverse Fourier transform on the result to obtain the high and low fluctuations of the rough surface. Due to the fact that rough surfaces are believed to be composed of a large amount of harmonic superposition, the amplitude of harmonics is an independent Gaussian random variable, and its variance is proportional to a specific power spectral density. The power spectrum corresponding to commonly used isotropic two-dimensional Gaussian rough surfaces is [38]

$$S(k_x, k_y) = \frac{\sigma_h^2 l^2}{4\pi} \exp\left(-\frac{k_x^2 l^2 + k_y^2 l^2}{4}\right) \tag{13}$$

Where, k_x and k_y represent the discrete wave numbers of the x-axis and y-axis, respectively, and the calculation formula is

$$k_x = \frac{2\pi N_x}{l}, \qquad k_y = \frac{2\pi N_y}{l} \tag{14}$$

Where, N_x and N_y are the equidistant scatter points of the x-axis and y-axis, respectively. The Fig.2 and Fig.3 show rough surfaces with root mean square heights of 0.1 mm and 0.5 mm, respectively, and corresponding distances of 5 mm, 10 mm, and 20 mm. From Fig.2 and Fig.3, it can be clearly seen that the root mean square height determines the height difference of the roughness surface undulations, and the correlation length determines the frequency of roughness surface undulations. For smooth surfaces, σ_h tends towards 0 and l tends towards infinity.

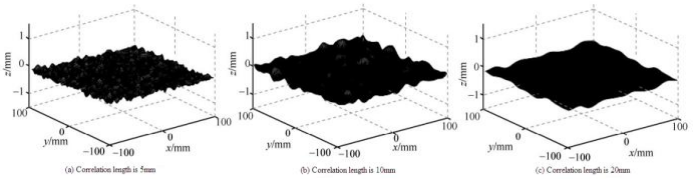

Fig.2. Rough surface with RMS height of 0.1mm

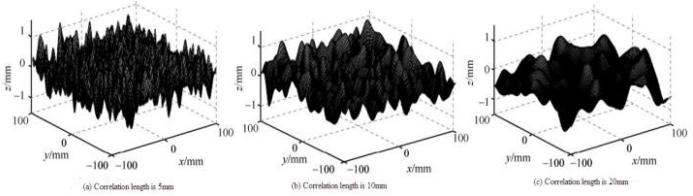

Fig.3. Rough surface with RMS height of 0.5mm

Designing experimental measurements is one of the most effective methods for studying the scattering characteristics of this new spectrum. Building high-precision measurement platforms and designing clever measurement schemes, conducting rigorous error analysis and correction, pose great challenges for the study of scattering characteristics. Based on electromagnetic calculation methods, exploring the scattering characteristics of the terahertz frequency band using classical electromagnetic theory is an effective alternative to experimental measurements. Comprehensive electromagnetic commercial software, such as X-Patch from the United States, FEKO jointly developed by Germany and South Africa, and CST from Germany, can achieve precise solution of complex surfaces. As an efficient method for sparsification of integral equations, the multi-level fast multipole method (MLFMM) is a multi-layer computational method that greatly improves the solving ability of numerical calculation methods. This part of the study utilized MLFMM in FEKO to simulate the rough surfaces of Figures 2 and 3, taking a perfect electric conductor (PEC) as an example. The incident wave is a plane wave that is obliquely incident on a rough surface at a 45° angle. Due to the different roughness of the material surface, the scattered energy is also different. The scattering of a rough surface with a root mean square height of 0.1 mm is shown in Fig.4.

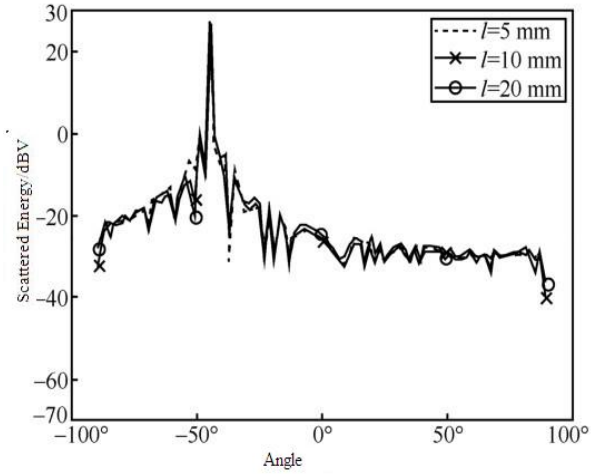

Fig.4. Scattering of rough surface with an RMS height of 0.1mm

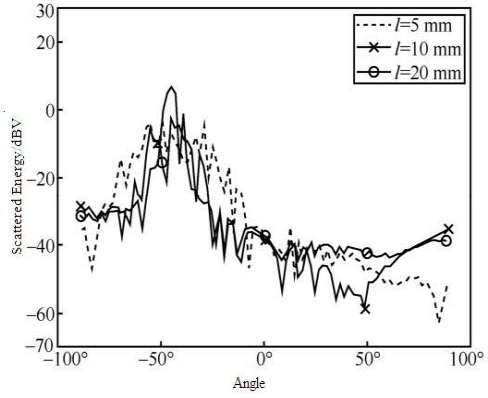

Fig.5. Scattering of rough surface with an RMS height of 0.5mm

The correlation distance l of the surface does not affect the shape of the scattering lobes, and the energy is concentrated in the direction of specular reflection. The scattering of a rough surface with a root mean square height of 0.5 mm is shown in Fig.5. As l decreases from 20 mm to 5 mm, it can be observed that the scattering lobes gradually increase and the electric field strength in the mirror reflection direction (-45 °) gradually decreases. Comparing the maximum values of the curves in Figures 4 and 5, it can be seen that the electric field strength in the mirror reflection direction (-45°) is much greater when σ_h is 0.1 mm than when σ h is 0.5 mm. However, after verification, the superposition of specular reflection and diffuse reflection energy is the same as the incident energy, satisfying the law of conservation of energy.

3. TERAHERTZ CHANNEL CHARACTER-ISTIC ANALYSIS FRAMEWORK

This paper focuses on the modeling of terahertz channels. Based on the unique propagation mechanism of terahertz electromagnetic waves, this paper implants their unique propagation characteristics into a radiation tracking simulator that has been validated multiple times in the millimeter wave frequency band, and establishes a radiation tracking simulation platform with a complete propagation mechanism; Construct a terahertz channel characteristic analysis method based on ray tracing simulation by combining channel measurement data. This framework mainly includes four parts: limited channel measurement, ray tracing simulation calibration, extensive ray tracing simulation, and channel key parameter extraction.

3.1 LIMITED CHANNEL MEASUREMENTS

The basic terahertz channel measurement methods are divided into using a vector network analyzer (VNA) and a channel detector, with the main difference being the measurement domain. VNA measures the channel transfer function (CTF) of sub narrowband in the frequency domain, and the CTF of the entire communication bandwidth is the set of all sub narrowband CTFs; Then perform inverse fast Fourier transform (IFFT) to obtain the corresponding channel impulse response CIR. The channel detector directly transmits an ultra wideband M-sequence and obtains the wideband CIR by autocorrelation with the received signal. These two measurement methods each have their own advantages and disadvantages [39]. For example, due to the use of precise calibration methods, the system noise for channel measurement using VNA is low, and the CTF of each sub narrowband is accurate, thus obtaining accurate CTF and CIR for the entire bandwidth. However, this frequency domain measurement method often takes a long time to measure and cannot perform dynamic measurements to capture, so the channel changes caused by the Doppler effect cannot be captured. Time domain channel detectors can support dynamic channel measurement and theoretically measure the dynamic changes of the channel. However, due to the large bandwidth and strong system thermal noise of terahertz measurement, as well as the limitations of current hardware equipment, it is not easy to capture useful multipath information. Therefore, regardless of which method is used, the data volume and degrees of freedom of terahertz channel measurement cannot be compared with Sub-6

GHz channels. Therefore, it is necessary to use calibrated ray tracing to expand channel data.

3.2 RAY-TRACING SIMULATION CALIBRATION

Ray tracing technology, as a deterministic channel modeling method, is increasingly prominent in 5G and 6G communication. Due to the fact that computational complexity has always been a bottleneck for ray tracing simulation in real-world scenarios, one effective solution is to deploy ray tracing simulators on high-performance computing (HPC) platforms, effectively accelerating computationally intensive tasks through parallel hardware technology. This article takes CloudRT, a self-developed ray tracing simulation platform based on HPC cloud computing, as an example.

Before conducting large-scale simulations using ray tracing simulation, it is necessary to implant the terahertz characteristics that distinguish it from low frequencies into a ray tracing simulator and calibrate it using limited channel measurements. According to the Fresnel reflection formula and roughness information, the energy of the reflection path depends not only on the geometric information of the environment, but also on the real and imaginary parts of the relative dielectric constant (ε'and ε"). Therefore, it is necessary to use the method of minimum error calibration to invert the relative dielectric constant of the material by comparing the difference between the reflection path and the ray tracing simulation. The initial value of the relative permittivity can be obtained through open literature review (such as metals, rubber [41], glass [42], and bricks [37,44]). Subsequently, the simulated annealing algorithm can be used to calibrate the relevant materials. In addition, the geometric features of the scene model also need to be calibrated; Otherwise, the time of arrival (ToA) of multipath in the measurement and simulation will not be consistent. After calibration, the ray tracing simulator can adopt a more flexible antenna deployment method; For outdoor scenes, different weather modules can be loaded to explore the impact of meteorological factors on the channel.

3.3 MASSIVE RAY-TRACING SIMULATIONS

Terahertz channel detection is usually achieved through directional antennas, and channel measurement in the global environment requires further use of the two-dimensional scanning mechanism of directional antennas, which is often time-consuming and labor-intensive. There are also problems such as high RF cable losses and insufficient actual cable length. Therefore, it is necessary to use calibrated ray tracing simulations to more comprehensively characterize the channel, which can effectively improve the degree of freedom and universality of scene settings and channels, as shown below.

- Support more flexible transmitter and receiver positions.
- Support more flexible antenna polarization combinations (any combination of vertical and horizontal polarization).
- Support more flexible antenna coupling methods (single transmitter single receiver, multiple transmitter multiple receiver, etc.).
- Support more flexible environment configuration (similar to measurement environments and similar materials).
- Support dual mobility (transmitter and receiver are movable, and scatterers are also movable).
- Support different outdoor weather conditions (atmosphere, fog, rain, snow).

3.4 CHANNEL KEY PARAMETER EXTRACTION

Based on a large number of ray tracing simulation results, the obtained channel characteristics can be comprehensively characterized. The characteristics of a channel mainly include path loss (PL), shadow fading (SF), root mean square delay spread (RMS DS), Rician K-factor (KF), angular spread (AS), cross polarization ratio (XPR), etc. For mobile channels, Doppler frequency shift and Doppler spread need to be extracted. These channel parameters will be fitted using a normal distribution.

4. INDOOR DESKTOP SHORT-RANGE TERAHERTZ CHANNEL CHARACTERISTICS

4.1 CHANNEL MEASUREMENT

Terahertz communication provides high-capacity wireless connectivity for devices. Compared to dynamic channels, static channel measurements and channel characteristics within the scene are the first step in modeling. Typical indoor short-range communication can occur on desks, enabling high-speed information exchange between devices. The channel measurement equipment mainly consists of two parts [18], namely a four port VNA and a pair of spread spectrum modules, which achieve radio wave propagation of 295-330 GHz through frequency doubling. The measurement is set at 5001 frequency points, with a corresponding sampling interval Δ f of 7 MHz. Under this configuration, the corresponding delay resolution is 0.029 ns, which is small enough to distinguish multipath in the channel. In addition, the corresponding maximum delay is 143 ns, which is large enough to capture the multipath components of the measurement channel. The half power beamwidth (HPBW) of the antenna used for measuring the transmitter and receiver is approximately 10 °, and the antenna gain is approximately 25 dBi. VNA is equipped with precise calibration accessories and methods. In this section, the measurement adopts the full dual port calibration method: short open load through (SOLT) calibration method, which is widely used, easy to master, suitable for most applications, and can provide excellent accuracy and repeatability. Calibration is used for the entire measurement system, including waveguides, spread spectrum modules, cables, and VNA itself.

4.2 RAY TRACING SIMULATOR CALIBRATION

According to the operation steps, it is necessary to calibrate the ray tracing simulator based on the measurement results and reflect the relevant electromagnetic parameters of the material according to the obvious reflection multipath. Reconstructed the measurement environment in SketchUp software; The simulation configuration is consistent with the measurement configuration, with 295-330 GHz and 5001 frequency points set as well; The radio wave propagation mechanism configured in the simulation is the LoS path and the highest 6th order reflection path. Setting the smooth metal optical surface as PEC, while considering the painted metal surface of the spread spectrum module as a hardware design for handheld mobile devices or laptops, requires

calibration of its electromagnetic parameters. The relative electromagnetic parameters of the calibrated painted metal surface are ε'=1.4 and ε''=10.71; The imaginary part value is significantly smaller than that of metal, indicating that the electromagnetic parameters of metal materials will be directly affected after painting. The comparison between the simulation results of ray tracing and the measurement results is shown in Fig.6. From Fig.6, it can be seen that the simulation results and measurement results of ray tracing have good consistency in terms of multipath delay and power: the average error of multipath delay is less than 0.1 ns; The average power error is less than 0.1 dB. In addition, according to the simulation results of ray tracing, the main multipath is the reflection from the surface of the spreading module; Due to the fact that the HPBW of the measuring antenna itself is only 10 °, the reflection path from the desktop cannot be captured during the measurement. Overall, the calibrated ray tracing simulator can accurately reproduce channel measurements, and the simulation and measurement results are consistent.

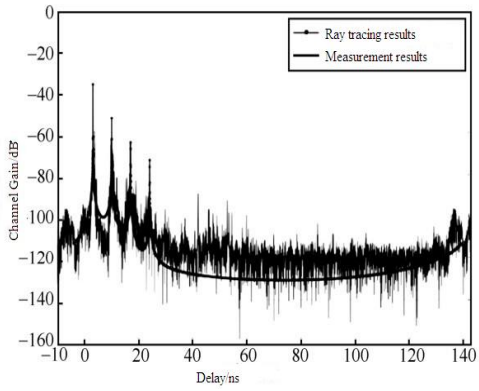

Fig.6. Comparison of ray tracing results and measurement results

4.3 EXTENSIVE RAY TRACING SIMULATIONS

In actual communication, users will place their mobile devices in different positions on the desktop. In the sub-6 GHz frequency band, comprehensive channel data can be obtained through a large amount of measured data. However, terahertz measurement is very limited by hardware equipment. A possible alternative method is to use ray tracing simulation for extensive simulation, and the placement of the transmitter and receiver should be more universal to generate rich channel impulse responses. In the simulation, the same system settings as the measurement will be used, with the transmitter placed on the left side of the desktop; In order to find the correlation between each position of the channel, the sampling interval of the receiver is set to 0.8 mm (less than the wavelength of the simulated frequency band), the communication range is set to 0.2-1.5 m, and the placement is shown in Fig.7. In addition, in order to compensate for the high path loss in the terahertz frequency band during measurement, the antenna uses a narrow beam high gain antenna, which cannot fully capture all multipath information in the environment. Therefore, using a calibrated ray tracing simulator, omnidirectional antennas can capture all multipath in the environment and obtain multi-dimensional channel information in the simulation.

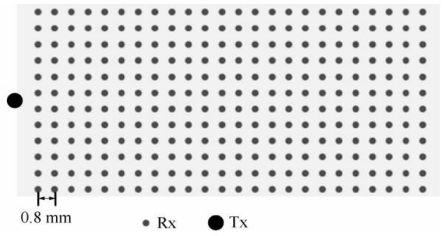

Fig.7. Schematic diagram of Tx and Rx positions in ray tracing

4.4 ANALYSIS OF CHANNEL CHARACTERISTICS

Based on a large number of ray tracing simulation results, the obtained channel characteristics can be comprehensively characterized. The characteristics of a channel mainly include path loss, root mean square delay spread, Rayleigh K-factor, angle spread, cross polarization rate, etc. These channel parameters will be fitted using a normal distribution function. Due to the scenario being defined as indoor short-range communication, molecular absorption attenuation and losses caused by fog, rain, and snow were not taken into account. The channel characteristics will be discussed in this section.

4.4.1 Path loss and Shadow Fading:

In this study, the A-B model was used for path loss, i.e.,

$$PL = A\log(d) + B + X_\sigma \tag{15}$$

Where, d is the distance between Tx and Rx; A is the slope of the fitted curve, B is the intercept; X_σ is shadow fading, which can be represented as a Gaussian distribution with a mean of 0 and a standard deviation of σ SF. The simulation results, fitting results, and comparison with free space losses of ray tracing are shown in Fig.8. The A value of the fitting result is 18.02, the B value is 81.71, and the σ SF value is 5.15 dB; The fitting curve almost overlaps with the free space loss curve, but from the simulation results, it can be seen that the simulation results fluctuate greatly. This is because using an omnidirectional antenna in the simulation can track the multipath in the entire scene. In addition to the reflection path of the device itself, it can also capture the strong reflection path from the desktop itself, so there is more multipath superposition in the propagation process.

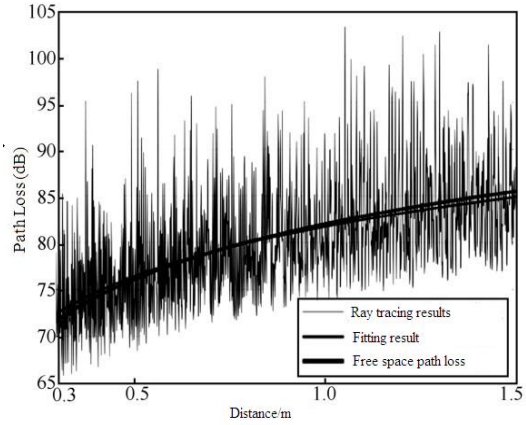

Fig.8.Ray tracing results, fitting results and comparison with free space loss

4.4.2 Rice K Factor and Root Mean Square Delay Extension

The Rice K factor quantifies the ratio of the strongest path to the sum of other multipath powers from a power perspective. The traditional method is to use the method of moments [44] to calculate from the narrowband channel detection results; The terahertz ultra wideband channel measurement and ray tracing simulation system have high time delay resolution in the time domain, and the Rayleigh K factor of each snapshot can be directly defined [45]

$$KF = \frac{P_d}{\sum(P(i) - P_d)} \tag{16}$$

Where, $P(i)$ is the energy of all multipath paths in the propagation process, and P_d is the energy of the direct path. The Fig.9 shows the comparison between ray tracing simulation and normal distribution fitting results, with a mean of 1.23 dB and a root mean square of 3.76 dB; Nearly 70% of the Rice K factor is greater than 0, indicating that although there are strong reflection paths from the desktop and the device itself in the scene, the direct reflection path still dominates. This is also a major feature of terahertz communication: compared to low-frequency communication scenarios, in the terahertz frequency band, the path loss of multipath is higher than that of direct path, which also causes multipath sparsity effect.

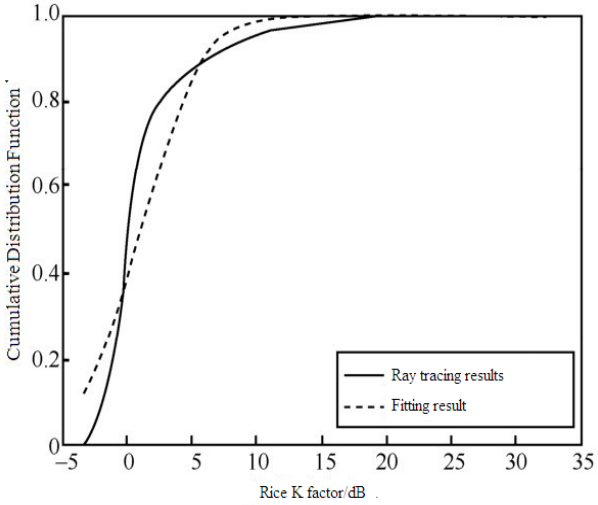

Fig.9. Comparison of ray tracing and normal distribution fitting results

Root mean square delay spread is a key parameter for effectively quantifying the dual dispersion effects of multipath channel power and time, defined as the square root of the second center distance of the delay power spectrum, i.e. [36]

$$\sigma_\tau = \sqrt{\frac{\sum_{n=1}^{N} \tau_n^2 P_n}{\sum_{n=1}^{N} P_n} - \left(\frac{\sum_{n=1}^{N} \tau_n P_n}{\sum_{n=1}^{N} P_n} \right)^2} \tag{17}$$

Where, P_n and τ_n respectively represent the power and delay of the nth multipath. The use of normal distribution can effectively perform data statistics on the root mean square delay spread of the entire scene, as shown in Fig.10. From Fig.10, it can be seen that the mean is 0.74 ns and the root mean square is 0.24 ns. This indicates that in short-range communication, even if there is a strong reflection path on a smooth plane, the relative delay caused by the reflection surface relative to LoS is small, and the root mean square delay spread value is also small. Compared to other wider scenarios in the same frequency band, such as in the intelligent high-speed railway scenario, the root mean square delay extension value obtained in a wide train station is relatively large, with an average of 6.61 ns [17].

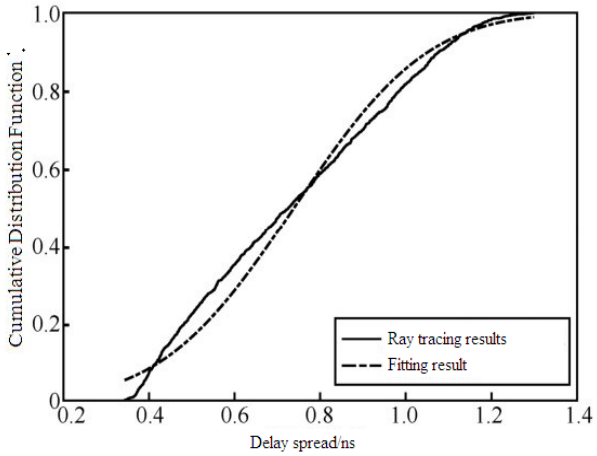

Fig.10. Delay spread statistics

4.4.3 Angle Expansion:

Angle extension defines the distribution of the arrival and departure angles of each multipath in the three-dimensional environment for Tx and Rx. The departure angle of each multipath at the transmitting end and the arrival angle at the receiving end will have a horizontal azimuth angle in the horizontal plane and an elevation angle in the vertical plane. Therefore, the angle extension includes four parameters: departure angle extension (ASD, azimuth angular spread of departure), departure angle extension (ESD, elevation angular spread of departure), arrival angle extension (ASA, azimuth angular spread of arrival), and arrival angle extension (ESA, elevation angular spread of arrival). The calculation equations are [46]

$$\sigma_{AS} = \sqrt{\frac{\sum_{n=1}^{N} (\theta_{n,\mu})^2 P_n}{\sum_{n=1}^{N} P_n}} \tag{18}$$

where, σ_{AS} represents angle extension, P_n represents the power and delay of the nth multipath; $\theta_{n,\mu}$ is defined as

$$\theta_{n,\mu} = \text{mod}(\theta_n - \mu_\theta + \pi, 2\pi) - \pi \tag{19}$$

where, θ_n is the corresponding pitch or horizontal departure or arrival angle of the n^{th} ray. The calculation formula for μ_θ is

$$\mu_\theta = \frac{\sum_{n=1}^{N} \theta_n P_n}{\sum_{n=1}^{N} P_n} \tag{20}$$

The Fig.11 and Fig.12 respectively show the extension of the departure angle at the transmitting end and the extension of the arrival angle at the receiving end. The horizontal angle expansion is mainly due to the placement of the receiver traversing the entire desktop, not just traversing the simulation along the centerline; When the device is offset from the transmitter position, the reflection path from the device itself will experience angular dispersion in the horizontal direction. The elevation angle

expansion mainly comes from the strong reflection path of the desktop. If the scenario is more general and the work is arranged on a wooden desktop instead of a simulated metal desktop, then there is usually not such a strong reflection path. Due to the fact that the materials in this scene are all smooth, scattering is not significant during propagation, while specular scattering satisfies equal angles of incidence and reflection. Therefore, the extension of the departure angle at the transmitting end is consistent with the extension of the arrival angle at the receiving end.

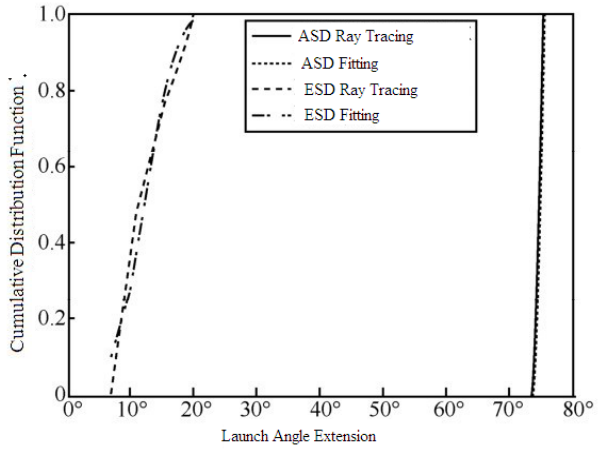

Fig.11. Transmitter departure angle expansion

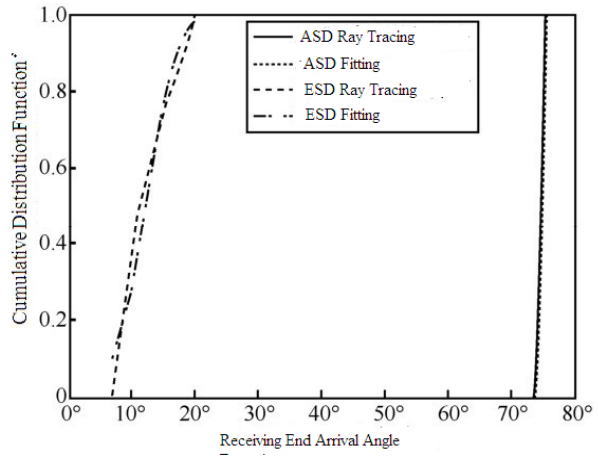

Fig.12. Receiver arrival angle expansion

4.4.4 Cross Polarization Rate:

Cross polarization rate is the ratio of the power in the maximum radiation direction of a given polarization to the power of the received orthogonal polarized wave in the secondary direction, used to measure the magnitude of its cross polarization component, which can be expressed as [47]

$$XPR = 10\log\left(\frac{P_{co}}{P_{cross}}\right) \tag{21}$$

The ratio of the received vertical (horizontal) co polarization (P_{co}) to the power of the transmission (P_{cross}) that sends vertical (horizontal) polarization and receives horizontal (vertical) polarization. As shown in Fig.13, $XPR > 0$. This indicates that there is almost no depolarization effect and that the scene is mainly dominated by direct radiation. Generally speaking, using a linearly polarized antenna at the transmitting and receiving ends in this scenario is sufficient, so a dual polarized antenna can be competent in this scenario. If there are more rough materials in the real scene, the depolarization effect will be enhanced, and circular polarization antennas should be considered.

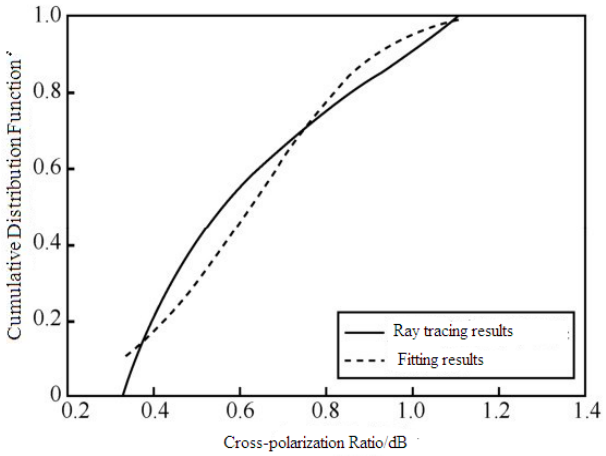

Fig.13. Cross polarization ratio

4.4.5 Summary of Channel Parameters:

In summary, the channel parameters of indoor short-range desktops were analyzed, and each parameter was analyzed using a normal distribution function for data statistics and parameter fitting, as shown in Table.1, where μ represents the mean and σ represents the standard deviation. The channel characteristics studied in this article can be used for link level and system level simulations to support terahertz indoor short-range communication.

Table.1. Parameters of Short-Range Indoor Terahertz Channel Characteristics

Parameters	μ	σ
KF/dB	1.31	3.86
DS/ns	0.81	0.03
ASD	75.77°	0.58°
ESD	13.23°	4.01°
ASA	75.77°	0.58°
ESA	13.23°	4.01°
APR/dB	8.52	4.45

5. CHANNEL CHARACTERISTICS OF HIGH-SPEED VEHICULAR NETWORKS

With the demand for high data rate communication services in intelligent vehicle networking, the hardware technology and wireless communication technology of automobiles will be closely integrated in the future, and intelligent transportation systems (ITS) will play an important role in modern transportation. When the vehicle is in high-speed autonomous driving mode, it must switch dynamic information in real time and quickly, and its communication link includes vehicle to vehicle (V2V), vehicle to infrastructure (V2I) and other vehicle to road cooperative communication. High speed movement will shorten

the time interval between spatial sampling points, which means that the multipath structure experienced by the channel at the same time will undergo drastic changes, and the channel will exhibit rapid and non-stationary characteristics. The assumption of generalized stationary uncorrelated scattering (WSSUS) used in traditional channels is no longer valid. Ray tracing technology can predict the multipath channel of each spatial sampling point with certainty, without using the assumption of generalized stationary non correlation. It can accurately characterize the channel characteristics under any high-speed movement, such as using low-speed movement measurements or even static measurement verification of ray tracing simulators, which can generate channel impulse responses under high-speed movement. Further extract mobile channel characteristics such as Doppler spread from the results. In addition, currently expensive terahertz measurement equipment is not suitable for conducting relevant measurements under adverse weather conditions. With the help of the meteorological factor module of ray tracing simulation, it can replace the measurement results of terahertz outdoor channels under different weather conditions.

5.1 PRELIMINARY MEASUREMENTS AND RAY-TRACING CALIBRATION

The preliminary work of this article [26,48] elaborated on the channel measurement experiments conducted in the context of the Internet of Vehicles. This experiment utilized an ultra wideband (UWB) channel detector capable of supporting measurements between 300-308 GHz to conduct two related terahertz channel measurements on an open railway testing center. The scene mainly includes major structures such as car bodies, lamp posts, and road surfaces, as well as major materials such as metal, glass, and brick. As described in Section 3, use measurement data to calibrate the material electromagnetic parameters and geometric information of the structure in the ray tracing simulator. The average error between the detected multipath in the first measurement and the multipath tracked by RT is 0.74 dB, and the average delay error is 0.19 ns, which means there is only a distance difference of 6 cm. In the second measurement, the average error of multipath power obtained from multipath measurement and ray tracing simulation was only 0.4 dB.

Table.2. Electromagnetic Parameters of Different Materials in Ray-Tracing Simulation

Material	Relative Permittivity	Conductivity (S/m)	S	α
Metal	1.001	1.1×10^7	0	0
Bricks	3.037	0.168	0.002	40
Glass	6.870	0.552	0.004	9

In addition, the electromagnetic parameters of relevant materials in the scene can also be obtained through inversion, as shown in Table.2 [48], which will be used for large-scale simulation using ray tracing technology in the next step. Where, ε 'and ε' 'represent the real and imaginary parts of the relative dielectric constant of the relevant material, respectively, and S and α represent the scattering factor and roughness equivalent factor of the material, respectively [49]. In addition, it can be inferred from the measurement and simulation tracking of multipath incoming wave directions that the metal vehicle body is the main reflector, which also proves that the vehicle body is a structural body with significant influence in subsequent terahertz channels.

5.2 RAY-TRACING SIMULATION FOR VEHICLE-TO-INFRASTRUCTURE (V2I) COMMUNICATION SCENARIOS

The calibrated ray tracing simulator can further support more flexible environmental configurations, such as environments similar to measurements and similar materials. This section will consider the simulation of vehicle networking channels in urban scenarios; In addition, based on the content of section 1.1, analyze the impact of different meteorological conditions on channel characteristics. The 3D scene considered in the simulation is constructed based on OpenStreetMap, and a four lane urban scene is selected as the target; The transmitter is set next to a traffic light at a height of 5 meters, and the receiver is mounted on a bus at a height of 3 meters. The simulation scene and the location of the transceiver are shown in Fig.14. The simulation frequency is 300-308 GHz, with 3201 frequency points, consistent with the measurement system parameters. In order to ensure that the simulation results are not affected by the antenna pattern and obtain a pure radio wave propagation channel, an omnidirectional vertically polarized antenna with zero transmission power and antenna gain is set at both the transmitting and receiving ends in the simulation.

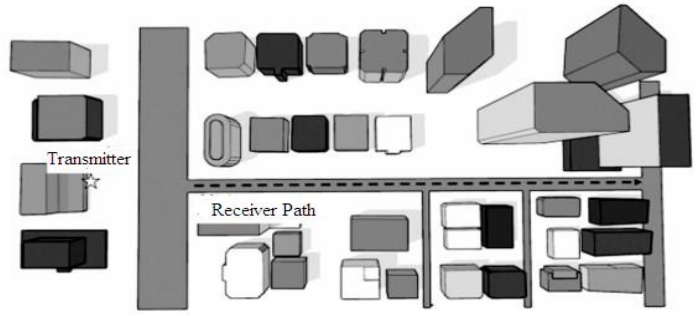

Fig.14. Simulation scenario and transceiver location

Section 2.1 of this article emphasizes that in the terahertz frequency band, atmospheric molecules and particles such as fog, rain, and snow cause attenuation of terahertz waves. Therefore, this article adopts the following steps to incorporate the attenuation caused by these factors into the simulation results.

Without considering the influence of meteorological factors, the CIR of any snapshot can be expressed as

$$h(\tau)=\sum_{n=1}^{N}E_n e^{j\phi}\delta(\tau-\tau_n) \tag{22}$$

where, n is the index of the ray (multipath), N is the total number of multipath in the snapshot, E_n, φ, and τ_n are the amplitude, phase, and delay of the ray electric field, respectively. Correspondingly, the power of the nth multipath that is not affected by meteorological factors is

$$P_n=20\log|E_n e^{j\phi}| \tag{23}$$

Then, add the meteorological attenuation an corresponding to the content in section 1.1 to the nth ray. So, CIR, which includes meteorological factors, is represented as

$$h_A(\tau) = \sum_{n=1}^{N} 10^{\frac{P_n - A_n}{20}} e^{j\phi} \delta(\tau - \tau_n) \quad (24)$$

Based on this, CIR can further analyze the channel characteristics containing different meteorological factors. In the 300 GHz frequency band, the attenuation caused by atmospheric gases, fog, rain, and snow is 5.2 dB/km, 7.26 dB/km, 21.42 dB/km (corresponding to precipitation R0.01=83.50 mm/h), and 350 dB/km, respectively.

5.3 CHANNEL CHARACTERISTIC ANALYSIS

5.3.1 Key Channel Parameters:

Based on a large number of RT simulation results and channel key parameter extraction methods similar to Section 3, as well as attenuation caused by different meteorological factors, the extraction data of key parameters for vehicle ground communication channels in the Internet of Vehicles, mainly including path loss, shadow fading, Rayleigh K factor, delay extension, and four angle extensions. Where, the parameters related to path loss (A, B, and σ SF) refer to equation (15); The remaining channel parameters are given by fitting the mean μ and standard deviation σ to a normal distribution. Previous studies usually only considered the received power under different meteorological environments, while this study emphasizes the influence of different meteorological factors on each channel parameter. The simulation data provided here is aimed at the question of how different meteorological conditions affect the performance of ground terahertz channels. Different from the relatively static channel characteristics, the key parameters of fast mobile communication, Doppler shift and extension, are detailed in the following text.

5.3.2 Doppler Shift and Doppler Spread:

For the vehicle to ground communication scenario, with a mobile receiver, the characteristics of Doppler effect can be analyzed based on multidimensional, comprehensive, and extensive simulation results. Due to the fact that the ray tracing simulator provides full dimensional information for each ray in each snapshot, it is possible to

To directly calculate the Doppler frequency shift of each ray according to the definition

$$f_d(n) = -\frac{f_c v_{R_x k(n)}}{c} \quad (25)$$

where, f_c is the center frequency; v_{Rx} is the speed of Rx; $k(n)$ is the unit vector of the nth ray starting from Tx and pointing towards the R_x direction from the scattering or reflection point; C is the speed of light.

Similar to the direct relationship between RMS delay spread and coherent channel, The RMS Doppler spread is related to the coherence time of the channel, representing the rate of change of the channel over time. It is characterized by the square root of the second centerdistance of the Doppler shift power spectrum

$$\sigma_v = \sqrt{\frac{\sum_{n=1}^{N} f_d(n)^2 P(n)}{\sum_{n=1}^{N} P(n)} - \left(\frac{\sum_{n=1}^{N} f_d(n) P(n)}{\sum_{n=1}^{N} P(n)} \right)} \quad (26)$$

where, $P(n)$ represents the power of the nth multipath. The Table.4 lists the maximum, average, and minimum Doppler frequency shifts of the entire scene, represented by μ. Since Doppler frequency shifts are independent of power attenuation, they are not affected by meteorological factors. At the same time, Table.3 lists the maximum, average, and minimum RMS Doppler spread of the entire scene under different meteorological conditions, represented by σ. If the 300 GHz vehicle networking system adopts orthogonal frequency division multiplexing technology, the subcarrier spacing should be greater than the maximum Doppler spread of 7.18 kHz. It is worth noting that the mean Doppler frequency shift is 17.63 kHz, which exceeds the Doppler frequency shift calibration capability of current 5G devices. Therefore, this parameter needs to be carefully considered when designing terahertz communication systems for vehicle networking.

Table.3. Doppler Shift and Doppler Spread

Parameter	μ_v/kHz	σ_v/kHz				
		RT	Atmosphere	fog	rain	snow
Maximum value	17.99	7.18	7.12	7.11	6.93	4.15
Mean	17.63	0.56	0.56	0.55	0.52	0.19
Minimum value	11.16	2.11	2.11	2.11	2.10	2.03

6. CONCLUSION

This article proposes a method for channel characteristic analysis based on ray tracing technology, which can achieve true terahertz channel data close to 6G even in the absence of extensive channel depth measurement, and thus perform channel characteristic analysis. Ray tracing technology is the equivalent of various accurate propagation mechanisms as rays, including direct, reflection, scattering, diffraction, and transmission, and tracks and predicts these rays in simulation. Therefore, this article first provides a detailed introduction to the new characteristics of radio wave propagation in the terahertz spectrum. An accurate radio wave propagation model is the basis of ray tracing simulation. Due to the absorption of terahertz radio wave energy by atmospheric molecules and the power attenuation caused by particle scattering effects of fog, rain, and snow, this article adds a meteorological prediction module to ray tracing technology; Due to the short wavelength of terahertz waves, the plane that was originally considered smooth at low frequencies is no longer smooth in the terahertz frequency band. Therefore, the anti scattering characteristics of terahertz wave propagation have been analyzed. Furthermore, this article proposes a method for correcting ray tracing simulators using a small amount of channel measurement data; At the same time, using a ray tracing simulator to invert relevant material parameters, and then conducting a large number of ray tracing simulations to obtain real and effective channel data; Extract key channel parameters from these channel data and analyze the channel characteristics of the target scenario. The two case studies proposed in this article are from indoor desktop communication scenarios to outdoor intelligent vehicle networking scenarios, representing both ends of 6G mobile communication from short distance to long distance use cases. For outdoor scenarios, the impact of different meteorological conditions on channel parameters is also considered, including path loss, shadow fading, root mean square delay extension, Rayleigh K factor, angle extension, cross polarization rate, etc.

Doppler frequency shift and Doppler extension need to be extracted for mobile channels. These key channel parameters are of great significance for the design and evaluation of terahertz systems.

The deterministic channel modeling method based on ray tracing can obtain comprehensive and fine channel spatial, temporal, frequency, and polarization information. This model has natural "spatial consistency" and requires high computational complexity for scene modeling, but can accurately characterize the complex multipath of the channel. The team in this article has a ray tracing simulator with completely independent intellectual property rights, which is installed on a high-performance computing platform. Public network access enables remote operation, greatly reducing computation time while ensuring modeling accuracy. At the same time, it breaks the long-term monopoly of European and American commercial software on this technology. Future work will continue to use radio wave propagation theory, channel measurement, and high-performance ray tracking as the main means to explore high-precision channel modeling methods in the terahertz frequency band based on mechanism models, serving the design, evaluation, and deployment of terahertz communication systems.

REFERENCES

[1] A. Ghosh, R. Ratasuk and B. Mondal, "LTE-Advanced: Next Generation Wireless Broadband Technology", *IEEE Wireless Communications*, Vol. 17, No. 3, pp. 10-22, 2010.

[2] B.P. Crow, I. Widjaja and J.G. Kim, "IEEE 802.11 Wireless Local Area Networks", *IEEE Communications Magazine*, Vol. 35, No. 9, pp. 116-126, 1997.

[3] T. Baykas, C.S. Sum and Z. Lan, "IEEE 802.15.3c: The First IEEE Wireless Standard for Data Rates Over 1 Gb/s", *IEEE Communications Magazine*, Vol. 49, No. 7, pp. 114-121, 2011.

[4] T.S. Rappaport, S. Sun and R. Mayzus, "Millimeter Wave Mobile Communications for 5G Cellular: It Will Work!", *IEEE Access*, Vol. 1, pp. 335-349, 2013.

[5] H. Elayan, O. Amin and B. Shihada, "Terahertz Band: The Last Piece of RF Spectrum Puzzle for Communication Systems", *IEEE Open Journal of the Communications Society*, Vol. 1, pp. 1-32, 2020.

[6] K. Guan, B. AI and B.L. Peng, "Towards Realistic High-Speed Train Channels at 5G Millimeter-Wave Band-Part I: Paradigm, Significance Analysis and Scenario Reconstruction", *IEEE Transactions on Vehicular Technology*, Vol. 67, No. 10, pp. 9112-9128, 2018.

[7] A. Fricke, S. Rey and B. Peng, "TG3D Channel Modelling Document", *IEEE Transactions on Vehicular Technology*, Vol. 63, No. 8, pp. 1-22, 2016.

[8] M. Narandzic, C. Schneider and R. Thoma, "Comparison of SCM, SCME and Winner Channel Models", *Proceedings of International Conference on Vehicular Technology*, pp. 413-417, 2007.

[9] J. Meinil, P. Kysti and T. JMS, "*Winner II Channel Models*", Technical Report, 2009.

[10] J. Bian, J. Sun and C.X. Wang, "A Winner+ based 3-D Non-Stationary Wideband MIMO Channel Model", *IEEE Transactions on Wireless Communications*, Vol. 17, No. 3, pp. 1755-1767, 2018.

[11] X. Cheng, Q. Yao and M.W. Wen, "Wideband Channel Modeling and Intercarrier Interference Cancellation for Vehicle-to-Vehicle Communication Systems", *IEEE Journal on Selected Areas in Communications*, Vol. 31, No. 9, pp. 434-448, 2013.

[12] S. Hur, Y.J. Cho and T. Kim, "Wideband Spatial Channel Model in an Urban Cellular Environment at 28 GHz", *Proceedings of International Conference on Antennas and Propagation*, pp. 1-5, 2015.

[13] T.S. Rappaport, G.R. Maccartney and M.K. Samimi, "Wideband Millimeter-Wave Propagation Measurements and Channel Models for Future Wireless Communication System Design", *IEEE Transactions on Communications*, Vol. 63, No. 9, pp. 3029-3056, 2015.

[14] C. YI and H. Chong, "Channel Modeling and Characterization for Wireless Networks-on-Chip Communications in the Millimeter Wave and Terahertz Bands", *IEEE Transactions on Molecular, Biological and Multi-Scale Communications*, Vol. 5, No. 1, pp. 30-43, 2019.

[15] Y.Z. Wu, J. Kokkoniemi and C. Han, "Interference and Coverage Analysis for Terahertz Networks with Indoor Blockage Effects and Line-of-Sight Access Point Association", *IEEE Transactions on Wireless Communications*, Vol. 20, No. 3, pp. 1472-1486, 2021.

[16] C. Yi and H. Chong, "Time-Varying Channel Modeling for Low-Terahertz Urban Vehicle-to-Infrastructure Communications", *Proceedings of International Conference on Global Communications*, pp. 1-6, 2019.

[17] K. Guan, D.P. He and B. Ai, "Channel Characterization and Capacity Analysis for THz Communication Enabled Smart Rail Mobility", *IEEE Transactions on Vehicular Technology*, Vol. 70, No. 5, pp. 4065-4080, 2021.

[18] H.F. Yi, K. Guan and D.P. He, "Terahertz Channel Measurement and Characterization on a Desktop from 75 to 400 GHz", *Proceedings of International Conference on Electronic Information and Communication Technology*, pp. 756-761, 2021.

[19] J.B. Fu, P. Juyal and A. Zajic, "THz Channel Characterization of Chip-to-Chip Communication in Desktop Size Metal Enclosure", *IEEE Transactions on Antennas and Propagation*, Vol. 67, No. 12, pp. 7550-7560, 2019.

[20] C.L. Cheng, S. Sangodoyin and A. Zajic, "THz Cluster-based Modeling and Propagation Characterization in a Data Center Environment", *IEEE Access*, Vol. 8, pp. 56544-56558, 2020.

[21] C.L. Cheng and A. Zajic, "Characterization of Propagation Phenomena Relevant for 300 GHz Wireless Data Center Links", *IEEE Transactions on Antennas and Propagation*, Vol. 68, No. 2, pp. 1074-1087, 2020.

[22] S. Hur, S. Baek and B. Kim, "Proposal on Millimeter-Wave Channel Modeling for 5G Cellular System", *IEEE Journal of Selected Topics in Signal Processing*, Vol. 10, No. 3, pp. 454-469, 2016.

[23] H. Chong and C. Yi, "Propagation Modeling for Wireless Communications in the Terahertz Band", *IEEE Communications Magazine*, Vol. 56, No. 6, pp. 96-101, 2018.

[24] S. Priebe, M. Kannicht and M. Jacob, "Ultra Broadband Indoor Channel Measurements and Calibrated Ray Tracing Propagation Modeling at THz Frequencies", *Journal of Communications and Networks*, Vol. 15, No. 6, pp. 547-558, 2013.

[25] Z.M. Yu, Y. Chen and G.J. Wang, "Wideband Channel Measurements and Temporal-Spatial Analysis for Terahertz Indoor Communications", *Proceedings of International Conference on Communications Workshops*, pp. 1-6, 2020.

[26] K. Guan, B.L. Peng and D.P. He, "Measurement, Simulation and Characterization of Train-to-Infrastructure Inside-Station Channel at the Terahertz Band", *IEEE Transactions on Terahertz Science and Technology*, Vol. 9, No. 3, pp. 291-306, 2019.

[27] K. Guan, H.F. Yi and D.P. He, "Towards 6G: Paradigm of Realistic Terahertz Channel Modeling", *China Communications*, Vol. 18, No. 5, pp. 1-18, 2021.

[28] G.A. Siles, J.M. Riera and P. Garcia-Del-Pino, "Atmospheric Attenuation in Wireless Communication Systems at Millimetre and THz Frequencies", *IEEE Antennas and Propagation Magazine*, Vol. 57, No. 1, pp. 48-61, 2015.

[29] International Telecommunication Union, "Attenuation by Atmospheric Gases and Related Effects", Available at https://www.itu.int/dms_pubrec/itu-r/rec/p/R-REC-P.676-13-202208-I!!PDF-E.pdf, Accessed in 2016.

[30] International Telecommunication Union, "Attenuation Due to Clouds and Fog", Available at https://www.itu.int/dms_pubrec/itu-r/rec/p/R-REC-P.840-7-201712-S!!PDF-E.pdf, Accessed in 2017.

[31] International Telecommunication Union, "Specific Attenuation Model for Rain for Use in Prediction Methods", Available at https://www.itu.int/dms_pubrec/itu-r/rec/p/R-REC-P.838-3-200503-I!!PDF-E.pdf, Accessed in 2005.

[32] International Telecommunication Union, "Characteristics of Precipitation for Propagation Modelling", Available at https://img.antpedia.com/standard/files/pdfs_ora/20211231/ITU-R%20P.837-2017.pdf, Accessed in 2017.

[33] International Telecommunication Union, "Propagation Data and Prediction Methods Required for the Design of Terrestrial Line-of-Sight Systems", Available at https://www.itu.int/dms_pubrec/itu-r/rec/p/R-REC-P.530-17-201712-S!!PDF-E.pdf, Accessed in 2017.

[34] F. Norouziari, E. Marchetti and E. Hoare, "Low-THz Wave Snow Attenuation", *Proceedings of International Conference on Radar*, pp. 1-4, 2018.

[35] J.J. Ma, J. Adelberg and R. Shrestha, "The Effect of Snow on a Terahertz Wireless Data Link", *Journal of Infrared, Millimeter and Terahertz Waves*, Vol. 39, No. 6, pp. 505-508, 2018.

[36] T.S. Rappaport, "*Wireless Communications-Principles and Practice*", Pearson Publisher, 2002.

[37] R. Piesiewicz, C. Jansen and D. Mittleman, "Scattering Analysis for the Modeling of THz Communication Systems", *IEEE Transactions on Antennas and Propagation*, Vol. 55, No. 11, pp. 3002-3009, 2007.

[38] L. Guo, R. Wang and Z. Wu, "*Basic Theory and Method of Random Rough Surface Scattering*", Academic Press, 2010.

[39] B.L. Peng, K. Guan and A. Kuter, "Channel Modeling and System Concepts for Future Terahertz Communications: Getting Ready for Advances Beyond 5G", *IEEE Vehicular Technology Magazine*, Vol. 15, No. 2, pp. 136-143, 2020.

[40] D.P. He, B. Ai and K. Guan, "The Design and Applications of High-Performance Ray-Tracing Simulation Platform for 5G and Beyond Wireless Communications: A Tutorial", *IEEE Communications Surveys and Tutorials*, Vol. 21, No. 1, pp. 10-27, 2019.

[41] International Telecommunication Union, "Propagation Data and Prediction Methods for the Planning of Indoor Radiocommunication Systems and Radio Local Area Networks in the Frequency Range 300 MHz to 450 GHz", Available at https://standards.globalspec.com/std/13487739/itu-r-p-1238, Accessed in 2019.

[42] R. Piesiewicz, T. Kleine-Ostmann and N. Krumbholz, "Terahertz Characterisation of Building Materials", *Electronics Letters*, Vol. 41, No. 18, pp. 1-11, 2005.

[43] R. Piesiewicz, C. Jansen and S. Wietzke, "Properties of Building and Plastic Materials in the THz Range", *International Journal of Infrared and Millimeter Waves*, Vol. 28, No. 5, pp. 363-371, 2007.

[44] T. Zhou, C. Tao and S. Salous, "Channel Characterization in High-Speed Railway Station Environments at 1.89 GHz", *Radio Science*, Vol. 50, No. 11, pp. 1176-1186, 2015.

[45] L. Bernado, T. Zemen and F. Tufvesson, "Time and Frequency-Varying K-Factor of Non-Stationary Vehicular Channels for Safety-Relevant Scenarios", *IEEE Transactions on Intelligent Transportation Systems*, Vol. 16, No. 2, pp. 1007-1017, 2015.

[46] ETSI, "Spatial Channel Model for Multiple-Input Multiple-Output (MIMO) Simulations", Available at https://www.etsi.org/deliver/etsi_tr/125900_125999/125996/18.00.00_60/tr_125996v180000p.pdf, Accessed in 2003.

[47] D.P. He, K. Guan and A. Fricke, "Stochastic Channel Modeling for Kiosk Applications in the Terahertz Band", *IEEE Transactions on Terahertz Science and Technology*, Vol. 7, No. 5, pp. 502-513, 2017.

[48] H.F. Yi, K. Guan and D.P. He, "Characterization for the Vehicle-to-Infrastructure Channel in Urban and Highway Scenarios at the Terahertz Band", *IEEE Access*, Vol. 7, pp. 166984-166996, 2019.

[49] V. Degli-Esposti, F. Fuschini and E.M. Vitucci, "Measurement and Modelling of Scattering from Buildings", *IEEE Transactions on Antennas and Propagation*, Vol. 55, No. 1, pp. 143-153, 2007.